Solid State Communications 253 (2017) 51–56

Contents lists available at ScienceDirect

Solid State Communications

journal homepage: www.elsevier.com/locate/ssc

Communication

New two-dimensional boron nitride allotropes with attractive electronic and optical properties

Masoud Shahrokhi[a,*], Bohayra Mortazavi[b], Golibjon R. Berdiyorov[c]

[a] Université Paris-Est, Laboratoire Modélisation et Simulation Multi Echelle, MSME UMR 8208 CNRS, 5 bd Descartes, F-77454 Marne-la-Vallée, France
[b] Institute of Structural Mechanics, Bauhaus-Universität Weimar, Marienstr. 15, D-99423 Weimar, Germany
[c] Qatar Environment and Energy Research Institute, Hamad Bin Khalifa University, Qatar Foundation, Doha, Qatar

A B S T R A C T

Using first principles calculations, structural, electronic and optical properties of five new 2D boron nitride (BN) allotropes have been studied. The results exhibit that the cohesive energy for all these five new allotrope is positive such as all these systems are stable; therefore, it is possible to synthesize these structures in experiments. It is found that the band gap of all new 2D BN allotropes is smaller than the *h*-BN sheet. In our calculations the dielectric tensor is derived within the random phase approximation (RPA). Specifically, the dielectric function, refraction index and the loss function, of the 2D BN allotropes are calculated for both parallel and perpendicular electric field polarizations. The results show that the optical spectra are anisotropic along these two polarizations. The results obtained from our calculations are beneficial to practical applications of these 2D BN allotropes in optoelectronics and electronics.

1. Introduction

Recently, two-dimensional (2D) nanomaterials have captivated enormous significant amount of attention due to the surge in graphene research which opens an avenue for the development of 2D semiconductors for future multifunctional electronic and optoelectronic device applications [1,2]. The production of an isolated graphene sheet was realized by several experimental groups [3,4]. Graphene is ideal for thin-film transistors, transparent and conductive composites and electrodes, and photonics [5–7]. These properties make graphene an ideal optoelectronic material [8–10]. Another analogous two-dimensional nanostructure is hexagonal Boron Nitride sheet (*h*-BN sheet) [11–13]. The *h*-BN sheet has been successfully fabricated in experiments by controlled energetic electron irradiation through a layer-by-layer sputtering process [14,15]. In the past few years, BN sheet has aroused extensive research interest due to many intriguing properties such as high chemical stabilities [16], excellent mechanical properties [17] and high thermal conductivities [18,19]. The *h*-BN sheet is a wide band gap (4.71 eV) 2D nanomaterial [20]. Hence, the application of *h*-BN sheet in semiconductor devices requires a small band gap in order to switch the conductivity between on and off states. New physical and chemical approaches for decreasing the band gap in *h*-BN are under discussion. Li et al. showed that certain line defects can lead to tailor-made edges on *h*-BN sheets that can significantly reduce the band gap of the BN sheet [21]. Zhang et al. suggested that the embedded linear acetylenic chains can provide more flexibility for manipulation of the atomic and electronic properties of hexagonal boron nitride [22]. Moreover, fully hydrogenated *h*-BN sheet has recently been suggested as an semiconductor with a band gap of 3.33 eV [20]. The electronic structure of doped *h*-BN sheets with carbon atoms have also been calculated [23]. Their results show that substitution by carbon atoms in *h*-BN sheets can lead to a decreasing in electronic band gap. An alternative strategy can consist in stabilization of novel BN allotropes. Recently, Li et al. have carried out a detailed investigation on the pentagonal *penta*-B_xN_y nanosheets [24]. Their studies on the stabilities, electronic properties, and mechanical properties suggest *penta*-BN_2 as an attractive material to call for further studies on both theory and experiment. Enyashin et al. have studied structural and electronic properties for six various monolayered allotropes of graphene-like BN, which are composed of alternant B-N bonds and include the atoms of different hybridization types (sp^2, sp^2+sp^1, and sp^2+sp^3) by using the density-functional-based tight-binding (DFTB) method [25]. They found that all these allotropes are less stable than *h*-BN sheet, though, preserving their integrity during molecular-dynamics simulations. Furthermore, a novel BN allotrope (namely P-BN) based on P carbon structure, which is stable, transparent and superhard has been studied recently [26]. It is found that at pressures above 4 GPa, it becomes energetically preferred over h-BN.

* Corresponding author.
E-mail address: shahrokhimasoud37@gmail.com (M. Shahrokhi).

http://dx.doi.org/10.1016/j.ssc.2017.02.002
Received 24 December 2016; Received in revised form 26 January 2017; Accepted 5 February 2017
Available online 08 February 2017
0038-1098/

Using this ab initio global search approach, we will explore some new 2D BN allotropes and investigate their geometric, electronic and optical properties. The paper is organized as follows: In the next section, the details of the computational methods employed to compute the structural, electronic and optical properties are presented. In Section 3, the structural properties of all BN allotropes are described. Section 4 covers the electronic properties of these nanostructures. In Section 5, optical properties of these systems such as imaginary and real part of dielectric function, refraction index and electron energy loss function are discussed. In the last section we summarize our studies and present the conclusions.

2. Computational details

In the present work, DFT calculations have been performed by adopting the generalized gradient approximation of PBE functional [27] for the exchange-correlation potential and the projector augmented wave (PAW) [28] method as implemented in the Vienna *ab initio* simulation package (VASP) [29]. Electronic wave functions have been expanded using a plane-wave basis set with cut-off energy of 500 eV. For the Brillouin zone integration, a 18×18×1 Γ-centered Monkhorst-Pack [30] *k*-point mesh has been used to ensure converged structural and electronic results and 32×32×1 *k*-point grids have been necessary for computing optical properties. Periodic boundary conditions [31] (PBC) were used and an empty space of 20 Å was introduced in the direction perpendicular to the planes (z-direction), which ensures that the interaction between the periodic images of the sheet is negligible. Non-spin polarized DFT was used in all calculations. All the structures have been optimized using the conjugate gradient algorithm until the residual forces have become smaller than 10^{-5} eV/Å. The tetrahedron method with Blöchl corrections was employed for density of states (DOS) calculations [32]. After calculation of the electronic ground states, optical properties like imaginary and real parts of the dielectric function, refraction index and electron energy loss function of the considered materials have been investigated by using the random phase approximation (RPA) method [33]. The RPA calculations have taken local field effects into account.

3. Structural properties

In this section, the optimized structural data such as lattice parameters and cohesive energy for the different systems are presented. We will investigate the geometric and electronic properties of five 2D BN allotropes: two hexagonal and three tetragonal structures. The variety of these BN allotropes needs them to be named. We use the combination of their structural geometry and defects to name them: BN1 has a same structure of *h*-BN sheet with the pentagon–heptagon (5–7) defect and homoelemental N–N bonds in the structure; the structure of BN2 is similar to *h*-BN sheet with the 5–7 defect and homoelemental B–B bonds in the structure; BN3 is made of hexagons in the tetragonal lattice defected by the square-octagon pair (4–8); BN4 has a tetragonal lattice with the square-octagon pairs; BN5 is made of hexagons in the tetragonal lattice defected by the pentagon–heptagon pairs.

The BN1 and BN2 are based on the “Haeckelite” structure for carbon atoms discovered by Terrones et al. [34]. The difference between BN1 and BN2 is that the order of Boron and Nitrogen atoms are reversed. The BN3 structure is build according the “Biphenylene” carbon structure [35,36]. We also predicted the BN4 based on the “Octagraphene” as it was proposed by Sheng et al. [37]. Finally, we proposed the BN5 structure on the basis of “Phagraphene” which was found recently by Wang et al. [38]. The top views of the supercell of *h*-BN sheet and five BN allotropes are shown in Fig. 1. The primitive cell together with the lattice parameters of each structure is also specified in this figure. Table 1 presents the lattice parameters for all consider structures. The optimized lattice constant and the bond length for BN sheet are 2.505 Å and 1.446 Å, and are in a good agreement with previous results [19,39,40].

To evaluate the stabilities of the 2D BN allotropes, the cohesive energy per atom has been calculated as $E_{coh} = (\sum_i E_i - E_t)/n$, where E_t is the total energy per cell, E_i is the energy of the i-th isolated atom, and n is the total number of atoms per cell. Table 1 presents the cohesive energy of 2D BN structures. For all aforementioned systems the cohesive energy is positive such as all these systems are stable, therefore, it is possible to synthesize these five new allotropes in experiments. Our results show that these five new allotropes are less stable compared to *h*-BN sheet. Moreover, among the new allotropes the structures containing B-B or N-N bond (BN1, BN2 and BN5) are less stable than other structures. This can be explained by inspecting the electron density. Fig. 2 shows the electron density contour plots for *h*-BN sheet and five BN allotropes. It can be seen that due to repulsive forces between same atoms, the structures containing B-B or N-N bond are less stable than other structures.

4. Electronic properties

To compare the electronic properties of 2D BN allotropes with the *h*-BN sheet, the band structure and the total density of states (DOS) of these systems have been calculated. Fig. 3 shows the band structure for all aforementioned systems along the high symmetry directions. The first Brillouin zone for both hexagonal and tetragonal structures is shown as well. It is well visible that the both valence band maximum (VBM) and the conduction band minimum (CBM) of *h*-BN sheet occur along the *K*-point, resulting in a direct band gap. The band gap of *h*-BN sheet is 4.7 eV and is close to previous data [19,20,39]. Table 1 summarizes our results for the band gap values of 2D BN allotropes within PBE approach. The valence band maximum of BN1 and BN2 sheets occurs at the *Γ*-point. The conduction band minimum of BN1 is situated at the *K*-point while it located at *M*-point for BN2, resulting in an indirect band gap. The electronic band gap of BN1 and BN2 sheets is 2.45 and 1.83 eV, respectively, which is smaller than *h*-BN sheet. BN3 system has a direct gap of 3.18 eV at the *Γ*-point.

The CBM and VBM of BN4 sheet occur along the *M*-*Γ*-direction, resulting in a direct band gap. The value of band gap for BN4 sheet is 4.00 eV which is 0.70 eV smaller than *h*-BN sheet. The VBM of BN5 sheet occurs at the *Γ*-point, while the CBM is located at the *M*-point, resulting in an indirect band gap. The value of this indirect band gap is 2.65 eV. It is found that the band gap of all 2D BN allotropes is smaller than the band gap of *h*-BN sheet which shows that these materials may be applied in electronic and optoelectronic devices.

5. Optical properties

Since our electronic calculations in Section 4 indicated the band gap of 2D BN sheets is smaller than *h*-BN sheet, investigation optical properties of these materials is beneficial to practical applications of these nanostructures in optoelectronics and electronics. In this section applying the random phase approximation method [33], the optical properties of 2D BN allotropes, such as the imaginary and real part of dielectric function, refraction index and electron energy-loss spectrum (EELS) are calculated. The optical properties are determined by the dielectric function $\varepsilon(\omega) = \mathrm{Re}\,\varepsilon_{\alpha\beta}(\omega) + i\mathrm{Im}\varepsilon_{\alpha\beta}(\omega)$, which is mainly contributed from the electronic structures. The imaginary part of the dielectric function $\mathrm{Im}\varepsilon_{\alpha\beta}(\omega)$ could be obtained from the momentum matrix elements between the occupied and unoccupied wave functions within the selection rules [9,41]

$$\mathrm{Im}\varepsilon_{\alpha\beta}(\omega) = \frac{4\pi^2 e^2}{\Omega}\lim_{q\to 0}\frac{1}{|q|^2}\sum_{c,v,k} 2w_k\,\delta(\varepsilon_{ck} - \varepsilon_{vk} - \omega) \times \langle u_{ck+e_\alpha q}|u_{vk}\rangle\langle u_{ck+e_\beta q}|u_{vk}\rangle^* \quad (1)$$

where q is the Bloch vector of the incident wave and w_k the **k**-point

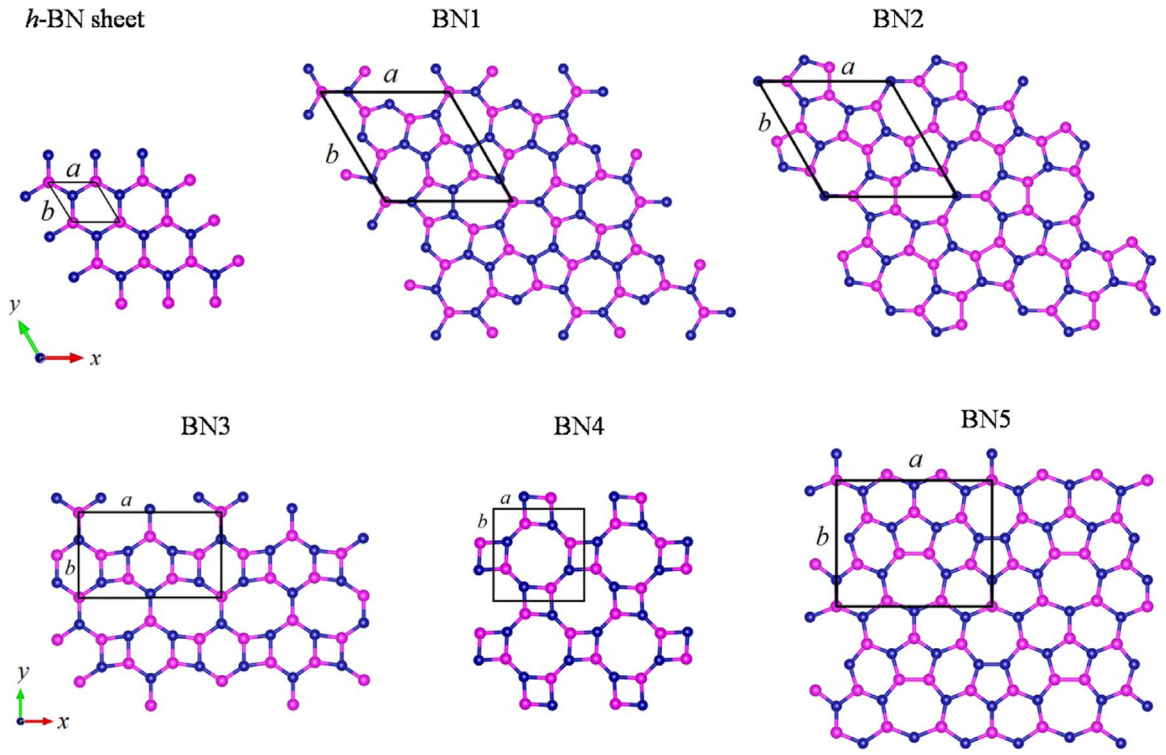

Fig. 1. Top view of optimized supercell structures of *h*-BN sheet and 2D BN allotropes. The primitive cell together with the lattice parameters of each structure is also shown. Dark blue and pink balls in the geometrical models represent the N and B atoms, respectively.

Table 1
Calculated lattice parameters, cohesive energy (E_{coh}) and electronic band gap of the 2D BN allotropes.

	Lattice parameters (Å) *ab*		E_{coh} (eV)	Band gap (eV)
BN sheet	2.505	2.505	8.77	4.70
BN1	7.141	7.141	8.43	2.45
BN2	7.390	7.390	8.05	1.83
BN3	7.655	4.557	8.50	3.20
BN4	4.934	4.934	8.47	4.00
BN5	8.311	6.736	8.45	2.65

weight. The band indices c and v are restricted to the conduction and the valence band states, respectively. The vectors e_α are the unit vectors for the three Cartesian directions and Ω is the volume of the unit cell. u_{ck} is the cell periodic part of the orbitals at the k-point **k**. The real part $\mathrm{Re}\,\varepsilon_{\alpha\beta}(\omega)$ can be evaluated from $\mathrm{Im}\varepsilon_{\alpha\beta}(\omega)$ using the Kramers–Kronig transformation [42,43]

$$\mathrm{Re}\,\varepsilon_{\alpha\beta}(\omega) = 1 + \frac{2}{\pi}P\int_0^\infty \frac{\omega'\mathrm{Im}\varepsilon_{\alpha\beta}(\omega')}{(\omega')^2 - \omega^2 + i\eta}d\omega' \quad (2)$$

where P denotes the principle value and η is the complex shift in Kramers-Kronig transformation. We have used a complex shift η=0.1 which is perfectly acceptable for most calculations and causes a slight smoothening of the real part of the dielectric function. Local field effects, which correspond to changes in the cell periodic part of the potential, were included in the RPA. All the other optical constants, such as refractive index n(ω), and energy-loss spectrum can be derived from $\mathrm{Re}\,\varepsilon_{\alpha\beta}(\omega)$ and $\mathrm{Im}\varepsilon_{\alpha\beta}(\omega)$[44]. In the present work, we report the optical properties of these compounds for parallel and perpendicular polarized directions ($E||x$ and $E||z$ from Fig. 1). Our results show that the optical spectra of BN1, BN2 and BN3 and BN5 systems are anisotropic for light polarizations along the x-axis ($E||x$) and y-axis ($E||y$) but there is a small difference in optical spectra along them, hence we just report the optical properties of these compounds for light polarizations along the x-axis. The imaginary and real parts of dielectric function of 2D BN allotropes for parallel and perpendicular polarized directions are illustrated in Fig. 4(a) and (b), respectively. As can be seen in these figures for parallel polarizations in the low-frequency regime, the absorption edge in imaginary part of dielectric constant of 2D BN allotropes shifted to the lower energies in comparison with h-BN sheet, this is known as red shift. The red shift values for perpendicular polarization are less than parallel polarization for these materials. Our results show that the first absorption peaks in imaginary part of dielectric constant for theses allotropes occur at energy range between 3 and 5 eV which are beneficial to practical applications in optoelectronic devices in the visible and ultraviolet spectral range. Moreover, there is a small peak in $\mathrm{Im}\varepsilon_{\alpha\beta}(\omega)$ of BN2 and BN5 in low frequency regime for $E||z$ which is completely missing in other allotropes. From Fig. 4 and Table 2 it is found that the static dielectric constant (the real part of dielectric constant at zero energy) increases for all 2D BN allotropes in parallel polarization in comparison with h-BN sheet. In perpendicular polarization, the static dielectric constant of BN2 and BN3 allotropes is greater than h-BN sheet while the static dielectric constant of BN1, BN4 and BN5 is smaller than h-BN sheet. In Fig. 4, the anisotropic response for parallel and perpendicular polarized directions to the planes can easily be observed for all these allotropes.

In the next step, we discussed the real part of refraction index for these nanostructures. The real part of refraction index is given by the following relation [45]

$$n_{ij}(\omega) = \sqrt{\frac{|\varepsilon_{ij}(\omega) + \mathrm{Re}\,\varepsilon_{ij}(\omega)|}{2}} \quad (3)$$

Fig. 5 shows the calculated the real part of refractive index of 2D BN allotropes for parallel and perpendicular polarized directions. The values of the static refraction index (the value of the refraction index at zero energy) of 2D BN allotropes increase in comparison with h-BN sheet for parallel polarization. Table 2 summarized the values of the static refraction index for all these materials. From Fig. 5 and Table 2 it is found that for perpendicular polarization the static dielectric constant for BN2 and BN3 allotropes slightly increases in comparison

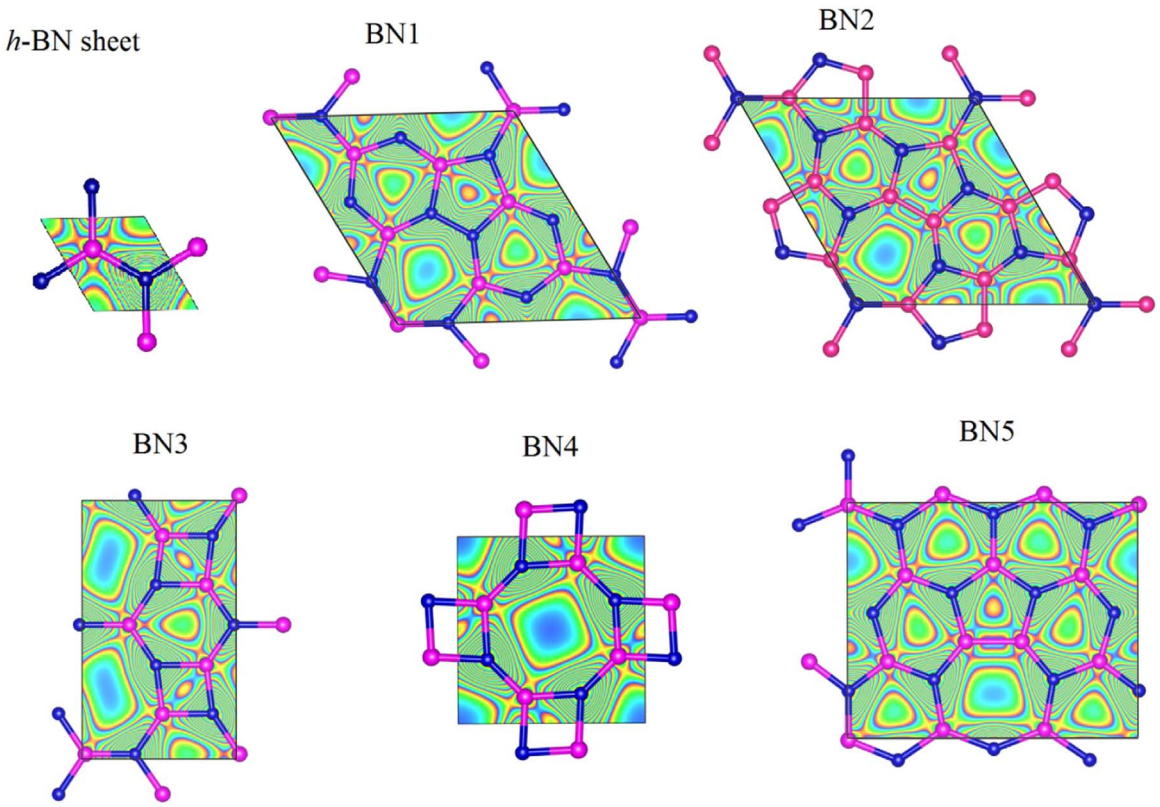

Fig. 2. 2D electron charge density distribution for *h*-BN sheet and 2D BN allotropes. Dark blue and pink balls in the geometrical models represent the N and B atoms, respectively.

with *h*-BN sheet, while for BN1, BN4 and BN5 it is decreased. The refractive index in $E||x$ ascends to the maximum value at4.56, 3.93, 3.85, 4.28, 4.09 and 2.73 eV for *h*-BN sheet, BN1, BN2, BN3, BN4 and BN5 allotropes, respectively. These energies in $E||z$ for the same cases are 9.67, 10.52, 9.21, 9.71, 9.78 and 10.03 eV.

In the last step, we discuss the electron energy loss spectra (EELS) of 2D BN allotropes. The EELS function has been calculated in terms of the real and the imaginary parts of the dielectric tensor, $\varepsilon_{\alpha\beta}(\omega)$, as defined by [44,46]

$$L_{\alpha\beta}(\omega) = -\mathrm{Im}\left(\frac{1}{\varepsilon_{\alpha\beta}(\omega)}\right) = \frac{\mathrm{Im}\varepsilon_{\alpha\beta}(\omega)}{(\mathrm{Re}\,\varepsilon_{\alpha\beta}(\omega))^2 + (\mathrm{Im}\varepsilon_{\alpha\beta}(\omega))^2} \tag{4}$$

The EELS is useful in revealing plasma resonance phenomena as distinct from normal interband transitions. In Fig. 6, the calculated EELS of all 2D BN allotropes for parallel and perpendicular polarized directions are plotted. Obvious, all these structures have two main peaks in the EELS spectra for parallel polarization. These main peaks in the energy-loss function are associated with the plasma oscillations.

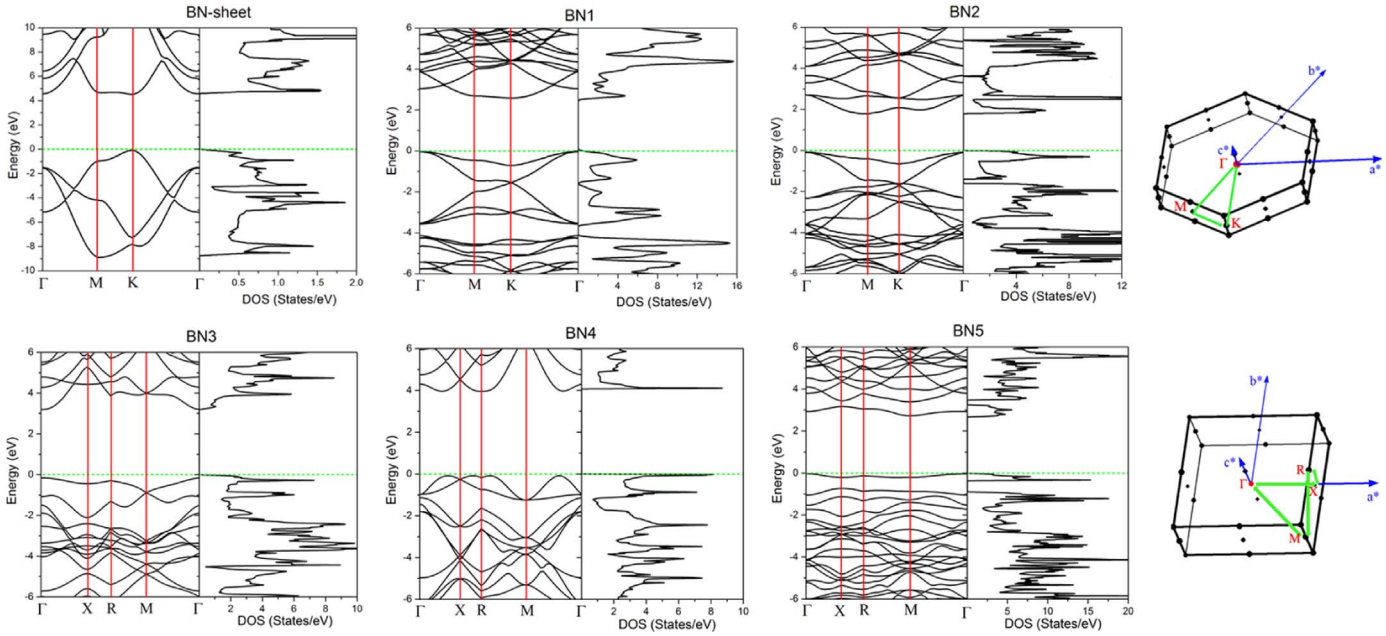

Fig. 3. Shows the band structure and corresponding total DOS of different 2D BN allotropes. The first Brillouin zone with *k*-path for energy band structure calculations for hexagonal (top) and tetragonal (bottom) lattices is illustrated.

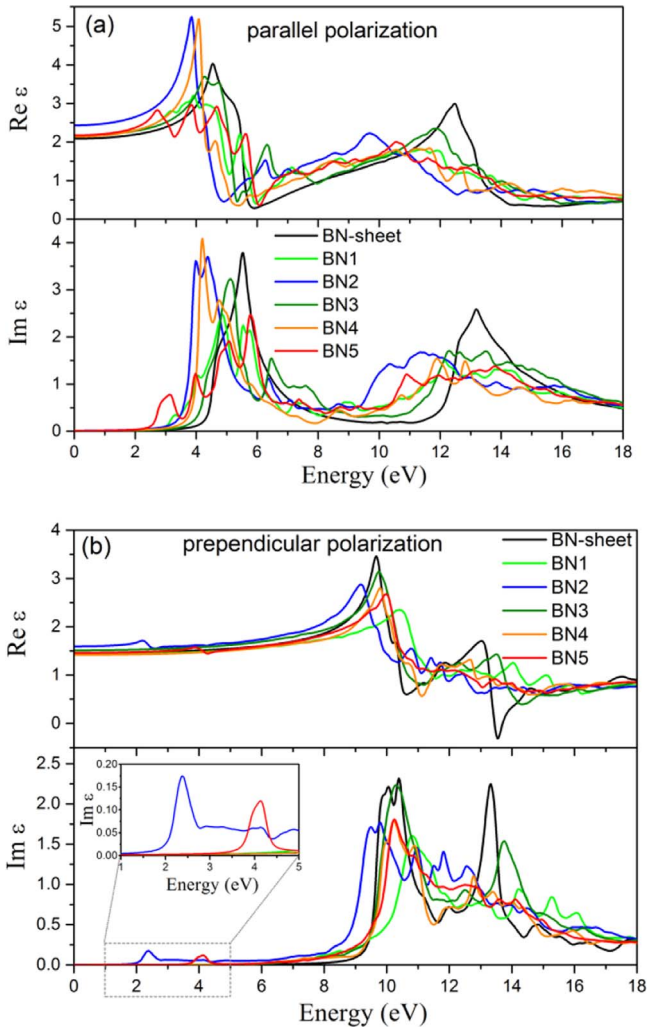

Fig. 4. Imaginary and real parts of the dielectric function of 2D BN allotropes for light polarizations (a) parallel to the *x*-axis and (b) perpendicular to the *x*-axis. Inset shows amplified regions of $\mathrm{Im}\varepsilon_{\alpha\beta}(\omega)$ in the low frequency regime for $E||z$.

Table 2
Calculated static dielectric constant ε (0), static refraction index n (0), first plasma frequency [First ω_p (eV)] and main plasma frequency [Main ω_p (eV)]of 2D BN allotropes for both polarizations, parallel and perpendicular to the plane.

	ε_{xx} (0) [ε_{zz} (0)]	n_{xx} (0) [n_{zz} (0)]	First ω_p (eV) xx [zz]	Main ω_p (eV) xx [zz]
h-BN sheet	2.09 [1.46]	1.44 [1.21]	4.86 [10.79]	16.83 [13.77]
BN1	2.15 [1.43]	1.47 [1.20]	4.06 [11.57]	17.59 [16.22]
BN2	2.43 [1.59]	1.56 [1.26]	4.09 [2.37]	17.4 [14.79]
BN3	2.16 [1.51]	1.47 [1.23]	4.5 [11.23]	17.29 [14.51]
BN4	2.14 [1.42]	1.46 [1.19]	4.42 [10.53]	18.49 [14.55]
BN5	2.17 [1.45]	1.47 [1.20]	3.2 [4.16]	18.22 [15.06]

Our calculated first peak and main peak plasma frequency for all BN allotropes are given in Table 2. The first plasmon peaks (which is due to plasma-oscillations of the π-electrons) for these allotropes appear around 5 eV in $E||x$ which shift to the lower energies in comparison with *h*-BN sheet. Furthermore, there is a small peak in EELS spectra of BN2 and BN5 at 2.37 and 4.16, respectively, for $E||z$ which is completely missing in other allotropes. Our results show that the main plasmon peaks for BN allotropes in both polarizations shift to the higher energies in comparison with *h*-BN sheet (Table 2). The main plasmon peak is due to plasma-oscillations of the $\pi+\sigma$ electrons.

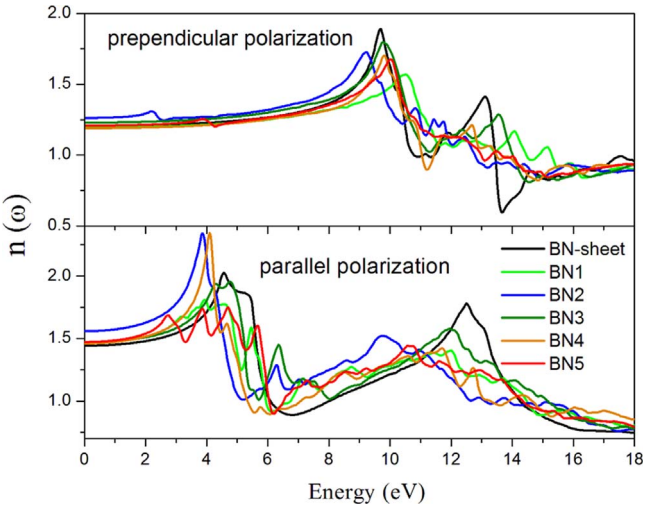

Fig. 5. Calculated real part of refraction index of 2D BN allotropes for parallel and perpendicular polarizations.

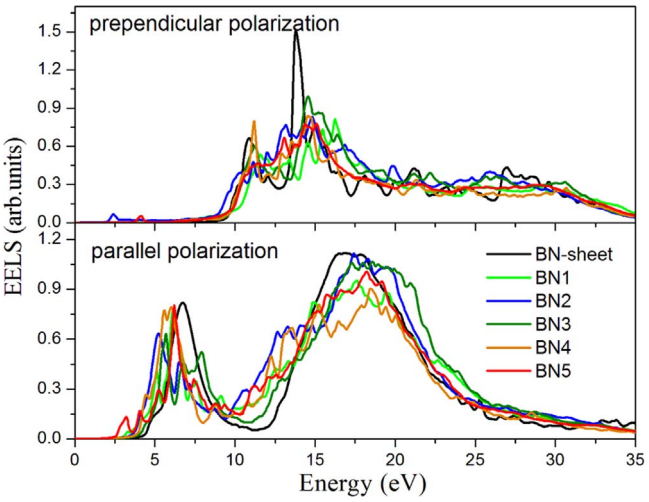

Fig. 6. The electron energy loss spectra of 2D BN allotropes for parallel and perpendicular polarizations.

6. Conclusions

In summary, using the *ab initio* global searches, we found five new 2D BN allotropes: two hexagonal and three tetragonal ones. First, the structural properties including lattice parameters and cohesive energy for all these systems have been calculated. Results show that due to positive cohesive energy for all these five new 2D BN allotropes all these systems are stable; therefore, it is possible to synthesize these allotropes in experiments. Because of repulsive forces between same atoms, the structures containing B-B or N-N bond are less stable than other structures. Moreover, these five new allotropes are less stable compared to *h*-BN sheet. The electronic results showed that the *h*-BN sheet is a direct band gap semiconductor with a band gap of 4.7 eV which both VBM and CBM occur at *K*-point. It is found that the band gap of new 2D BN allotropes is smaller than the band gap of *h*-BN sheet which shows that these materials may be applied in electronic and optoelectronic devices. The linear photon energy-dependent complex dielectric functions and related optical properties including refraction index and electron energy-loss spectrum were computed and discussed. Our results showed that for both polarizations in the low-frequency regime, the absorption edge in imaginary part of dielectric constant of 2D BN allotropes shifted to the lower energies in comparison with *h*-BN sheet. Moreover, the static dielectric constant and static refraction

index increase for all 2D BN allotropes in parallel polarization in comparison with *h*-BN sheet. It is found that the main plasmon peaks for BN allotropes in both polarizations shift to the higher energies in comparison with *h*-BN sheet. Our investigations are beneficial to the practical applications of these 2D BN allotropes in optoelectronics and electronics.

References

[1] Z. Wang, et al., Electronic and optical properties of novel carbon allotropes, Carbon 101 (2016) 77–85.
[2] M.J. Allen, V.C. Tung, R.B. Kaner, Honeycomb carbon: a review of graphene, Chem. Rev. 110 (1) (2010) 132–145.
[3] H.C. Schniepp, et al., Functionalized single graphene sheets derived from splitting graphite oxide, J. Phys. Chem. B 110 (17) (2006) 8535–8539.
[4] C. Berger, et al., Ultrathin Epitaxial graphite: 2D electron gas properties and a route toward graphene-basedgraphene-based nanoelectronics, J. Phys. Chem. B 108 (52) (2004) 19912–19916.
[5] J.S. Bunch, et al., Electromechanical resonators from graphene sheets, Science 315 (5811) (2007) 490–493.
[6] Z. Sun, et al., Graphene mode-lockedmode-locked ultrafast laser, ACS Nano 4 (2) (2010) 803–810.
[7] R. Moradian, M. Shahrokhi, S. Moradian, First principle study of the structural, electronic and magnetic properties of Fe, Co, Ni atomic nanochains encapsulated in single walled and double walled beryllium oxygen nanotubes, Physica E: Low-Dimens. Syst. Nanostruct. 47 (2013) 40–45.
[8] A.G. Marinopoulos, et al., *Ab initio* study of the optical absorption and wave-vector-dependent dielectric response of graphite, Phys. Rev. B 69 (24) (2004) 245419.
[9] M. Shahrokhi, C. Leonard, Tuning the band gap and optical spectra of silicon-doped graphene: many-body effects and excitonic states, J. Alloy. Compd. 693 (2017) 1185–1196.
[10] A. Esmailian, M. Shahrokhi, F. Kanjouri, Structural, electronic and magnetic properties of (N, C)-codoped ZnO nanotube: first principles study, Int. J. Mod. Phys. C 26 (11) (2015) 1550130.
[11] A. Fathalian, R. Moradian, M. Shahrokhi, Optical properties of BeO nanotubes: ab initio study, Solid State Commun. 156 (2013) 1–7.
[12] S. Naderi, et al., Structural, electronic and magnetic properties of Fe and Co monatomic nanochains encapsulated in BN nanotube bundle, Eur. Phys. J. Appl. Phys. 62 (3) (2013) 30402.
[13] M. Shahrokhi, R. Moradian, Structural, electronic and magnetic properties of Fe, Co, Ni monatomic nanochains encapsulated in BeO nanotubes bundle, Eur. Phys. J. Appl. Phys. 65 (2) (2014) 20402.
[14] C. Jin, et al., Fabrication of a freestanding boron nitride single layer and its defect assignments, Phys. Rev. Lett. 102 (19) (2009) 195505.
[15] J.C. Meyer, et al., Selective sputtering and atomic resolution imaging of atomically thin boron nitride membranes, Nano Lett. 9 (7) (2009) 2683–2689.
[16] D. Golberg, et al., Boron nitride nanotubes and nanosheets, ACS Nano 4 (6) (2010) 2979–2993.
[17] L. Chun, et al., Thickness-dependent bending modulus of hexagonal boron nitride nanosheets, Nanotechnology 20 (38) (2009) 385707.
[18] M.L. Hu, et al., Tunneling magnetoresistance of bilayer hexagonal boron nitride and its linear response to external uniaxial strain, J. Phys. Chem. C 115 (16) (2011) 8260–8264.
[19] R. Moradian, et al., Structural, magnetic, electronic and optical properties of iron cluster (Fe6) decorated boron nitride sheet, Physica E: Low-Dimens. Syst. Nanostruct. 46 (2012) 182–188.
[20] J. Zhou, et al., Electronic and magnetic properties of a BN sheet decorated with hydrogen and fluorine, Phys. Rev. B 81 (8) (2010) 085442.
[21] X. Li, et al., Band-gap engineering via tailored line defects in boron-nitride nanoribbons, sheets, and nanotubes, ACS Nano 6 (5) (2012) 4104–4112.
[22] H. Zhang, et al., Flexible band gap tuning of hexagonal boron nitride sheets interconnected by acetylenic bonds, Phys. Chem. Chem. Phys. 17 (31) (2015) 20376–20381.
[23] N. Berseneva, et al., Electronic structure of boron nitride sheets doped with carbon from first-principles calculations, Phys. Rev. B 87 (3) (2013) 035404.
[24] J. Li, et al., Penta-BxNy sheet: a density functional theory study of two-dimensional material, Sci. Rep. 6 (2016) 31840.
[25] A.N. Enyashin, A.L. Ivanovskii, Graphene-like BN allotropes: structural and electronic properties from DFTB calculations, Chem. Phys. Lett. 509 (4–6) (2011) 143–147.
[26] J. Xue, Z. Jijun, A. Rajeev, A novel superhard BN allotrope under cold compression of h-BN, J. Phys. Condens. Matter 25 (12) (2013) 122204.
[27] J.P. Perdew, K. Burke, M. Ernzerhof, Generalized gradient approximation made simple, Phys. Rev. Lett. 77 (18) (1996) 3865–3868.
[28] G. Kresse, D. Joubert, From ultrasoft pseudopotentials to the projector augmented-wave method, Phys. Rev. B 59 (3) (1999) 1758–1775.
[29] G. Kresse, J. Furthmüller, Efficient iterative schemes for ab initio total-energy calculations using a plane-wave basis set, Phys. Rev. B 54 (16) (1996) 11169–11186.
[30] H.J. Monkhorst, J.D. Pack, Special points for Brillouin-zone integrations, Phys. Rev. B 13 (12) (1976) 5188–5192.
[31] G. Makov, M.C. Payne, Periodic boundary conditions in *ab initio* calculations, Phys. Rev. B 51 (7) (1995) 4014–4022.
[32] P.E. Blöchl, O. Jepsen, O.K. Andersen, Improved tetrahedron method for Brillouin-zone integrations, Phys. Rev. B 49 (23) (1994) 16223–16233.
[33] M. Gajdoš, et al., Linear optical properties in the projector-augmented wave methodology, Phys. Rev. B 73 (4) (2006) 045112.
[34] H. Terrones, et al., New metallic allotropes of planar and tubular carbon, Phys. Rev. Lett. 84 (8) (2000) 1716–1719.
[35] F. Schlütter, et al., Octafunctionalized biphenylenes: molecular precursors for isomeric graphene nanostructures, Angew. Chem. Int. Ed. 53 (6) (2014) 1538–1542.
[36] O. Rahaman, et al., Metamorphosis in carbon network: from penta-graphene to biphenylene under uniaxial tension, FlatChem 1 (2017) 65–73.
[37] X.-L. Sheng, et al., Octagraphene as a versatile carbon atomic sheet for novel nanotubes, unconventional fullerenes, and hydrogen storage, J. Appl. Phys. 112 (7) (2012) 074315.
[38] Z. Wang, et al., Phagraphene: a low-energy graphene allotrope composed of 5–6–7 carbon rings with distorted Dirac cones, Nano Lett. 15 (9) (2015) 6182–6186.
[39] M. Kan, et al., Tuning the band gap and magnetic properties of BN sheets impregnated with graphene flakes, Phys. Rev. B 84 (20) (2011) 205412.
[40] S. Tang, S. Zhang, Electronic and magnetic properties of hybrid boron nitride nanoribbons and sheets with 5–7 line defects, J. Phys. Chem. C 117 (33) (2013) 17309–17318.
[41] M. Shahrokhi, S. Naderi, A. Fathalian, Ab initio calculations of optical properties of B2C graphene sheet, Solid State Commun. 152 (12) (2012) 1012–1017.
[42] M. Shahrokhi, Quasi-particle energies and optical excitations of ZnS monolayer honeycomb structure, Appl. Surf. Sci. 390 (2016) 377–384.
[43] M. Shahrokhi, C. Leonard, Quasi-particle energies and optical excitations of wurtzite BeO and its nanosheet, J. Alloy. Compd. 682 (2016) 254–262.
[44] R. Moradian, M. Shahrokhi, Structural, electronic and optical properties of nanotubes: first principles study, J. Phys. Chem. Solids 74 (8) (2013) 1063–1068.
[45] M. Shahrokhi, R. Moradian, Structural, electronic and optical properties of Zn1−xZrxO nanotubes: first principles study, Indian J. Phys. 89 (3) (2015) 249–256.
[46] R. Moradian, M. Shahrokhi, First principles study of the structural, electronic and optical properties of nanotube, Physica E: Low-Dimens. Syst. Nanostruct. 44 (7–8) (2012) 1760–1765.